

**Reduced nicotinamide adenine
dinucleotide fluorescence lifetime detected
poly(adenosine-5'-diphosphate-ribose)
polymerase-1-mediated cell death and
therapeutic effect of pyruvate**

Han-Wen Guo
Yau-Huei Wei
Hsing-Wen Wang

Reduced nicotinamide adenine dinucleotide fluorescence lifetime detected poly(adenosine-5'-diphosphate-ribose) polymerase-1-mediated cell death and therapeutic effect of pyruvate

Han-Wen Guo,^a Yau-Huei Wei,^{b,c} and Hsing-Wen Wang^a

^aNational Yang-Ming University, Institute of Biophotonics, Taipei 112, Taiwan

^bNational Yang-Ming University, Institute of Biochemistry and Molecular Biology, Taipei 112, Taiwan

^cMackay Medical College, Department of Medicine, SanJhjh, Taipei County 252, Taiwan

Abstract. Noninvasive detection of cell death has the potential for definitive diagnosis and monitoring treatment outcomes in real time. Reduced nicotinamide adenine dinucleotide (NADH) fluorescence intensity has long been used as a noninvasive optical probe of metabolic states. NADH fluorescence lifetime has recently been studied for its potential as an alternative optical probe of cellular metabolic states and cell death. In this study, we investigated the potential using NADH fluorescence intensity and/or lifetime to detect poly(adenosine-5'-diphosphate-ribose) polymerase-1 (PARP-1)-mediated cell death in HeLa cells. We also examined if NADH signals respond to treatment by pyruvate. The mechanism of PARP-1-mediated cell death has been well studied that extensive PARP-1 activation leads to cytosolic nicotinamide adenine dinucleotide depletion resulting in glycolytic inhibition, mitochondrial failure, and death. Pyruvate could restore electron transport chain to prevent energy failure and death. Our results show that NADH fluorescence lifetime, not intensity, responded to PARP-1-mediated cell death and the rescue effect of pyruvate. This lifetime change of NADH fluorescence happened before the collapse of mitochondrial membrane potential and mitochondrial uncoupling. Together with our previous findings in staurosporine-induced cell death, we suggest that NADH fluorescence lifetime increase during cell death is mainly due to increased protein-protein interactions but not the intracellular NADH content. © 2011 Society of Photo-Optical Instrumentation Engineers (SPIE). [DOI: 10.1117/1.3590204]

Keywords: reduced nicotinamide adenine dinucleotide fluorescence intensity and lifetime; poly(adenosine-5'-diphosphate-ribose) polymerase-1-mediated cell death; mitochondrial functions.

Paper 11029R received Jan. 17, 2011; revised manuscript received Apr. 8, 2011; accepted for publication Apr. 11, 2011; published online Jun. 9, 2011.

1 Introduction

The poly[adenosine-5'-diphosphate (ADP)-ribose] polymerase-1 (PARP-1) is a nuclear enzyme involved in various biological processes such as DNA repair, gene expression, and genomic stability. When PARP-1 is activated by DNA damage for example, nicotinamide adenine dinucleotide (NAD⁺) and adenosine-5'-diphosphate (ADP) were used to form poly(ADP-ribose).¹ Excessive PARP-1 activation can significantly deplete cytosolic NAD⁺ and subsequently cause energy deficiency that lead to cell death.²⁻⁴ Following this NAD⁺ depletion, adenosine-5'-triphosphate (ATP) depleted for NAD⁺ resynthesis,⁵ glycolysis was inhibited,⁶ and/or PAR over-expressed to trigger apoptosis-induced factor from mitochondria to the nucleus.⁷

PARP-1-mediated cell death occurs in many diseases including brain ischemia, trauma, myocardial infarction, and inflammatory injury.^{2,8} To restore the energy failure and rescue the cells from death, scientists have succeeded in the use of pyruvate, a glycolytic product, that does not require cytosolic NAD⁺ for energy metabolism but force mitochondria to resume the electron transport chain and generate ATP.^{6,9,10} Alternatively, direct

application of NAD⁺ or reduced nicotinamide adenine dinucleotide (NADH) has been shown to prevent PARP-1-mediated cell death by resuming the flux of glucose-derived pyruvate and NADH to enter mitochondria for oxidative metabolism.^{11,12}

Noninvasive detection of cell death has the potential for effective diagnosis of the disease and monitoring of the treatment outcome in real time. NADH fluorescence intensity is a widely accepted noninvasive optical probe of the metabolic state in mitochondria. Decreased NADH fluorescence intensity was detected during cell death *in vitro* and *in vivo*.^{13,14} The lifetime parameters of NADH fluorescence have recently been investigated for its potential use as the biomarker of cell metabolic states and death. NADH fluorescence lifetime usually refers to its mean lifetime ($\tau_m = a_1\tau_1 + a_2\tau_2$) where τ_1 is free NADH fluorescence lifetime ($\tau_1 \sim 400$ to 500 ps), τ_2 is bound NADH fluorescence lifetime ($\tau_2 \sim 2000$ to 3000 ps), a_1 and a_2 are the corresponding amplitudes.^{15,16} Studies by other groups and our laboratory have shown that NADH fluorescence lifetime is associated with the metabolic state of cells¹⁶⁻¹⁸ and staurosporine (STS)-induced mitochondria-mediated cell death,¹⁹ respectively. However, no other cell death model has been used to demonstrate if the NADH fluorescence lifetime responds the same as we previously showed in STS-induced cell death.

Address all correspondence to: Hsing-Wen Wang, National Yang-Ming University, Institute of Biophotonics, 155 Li-Nong Street, Sec. 2, Taipei 112, Taiwan. Tel: 886-2-2826-7378; Fax: 886-2-2823-5460; E-mail: hwwang2@ym.edu.tw.

We aimed to broaden our investigation to noninvasively detect cell death using NADH fluorescence lifetime as an optical probe. We chose PARP-1-mediated cell death in this study because it occurred in ischemia and several human diseases. Once we demonstrate that the NADH fluorescence signal responds to cell death and the treatment of disease, we can directly extend this measurement scheme into clinical applications. Second, the mechanism of PARP-1-mediated cell death has been well documented and its pathway is directly involved with NAD⁺ and/or NADH. Thus, the origin of the NADH fluorescence signal change may be better understood in this case. We used an alkylating agent, N-methyl-N'-nitro-N-nitrosoguanidine (MNNG), to activate PARP-1 as described in several other studies.^{4,6,9,11,12} The time course of NADH fluorescence lifetime and intensity micrographs of HeLa cells were acquired after MNNG treatments to compare with the time course of mitochondrial functions, including mitochondrial membrane potential ($\Delta\Psi$), ATP level, and oxygen consumption. Pyruvate was then used to restore the electron transport chain after the washout of 30 min MNNG exposure. In parallel, the glycolytic substrate glucose, which was reported to have no effect in restoration of PARP-1-induced energy failure,⁹ was used to treat a separate group of cells after the washout of MNNG exposure for 30 min. NADH fluorescence lifetime and intensity of treated cells with pyruvate or glucose were then measured and the results were compared with those cells treated with MNNG only. Our results indicate that NADH fluorescence lifetime, not the fluorescence intensity of NADH, could be an optical biomarker for detecting PARP-1-mediated cell death and monitoring the therapeutic outcome. The NADH fluorescence lifetime increased soon after 100 μM MNNG treatment of HeLa cells and before mitochondrial membrane potential depletion and mitochondrial uncoupling, and it was dependent on MNNG concentration. Furthermore, the results of cellular NADH content and NADH fluorescence intensity measurements suggest that NADH had mainly remained in the mitochondria after MNNG treatment. The remaining NADH molecules may have played an important role in the determination of cell survival upon addition of pyruvate.

2 Materials and Methods

2.1 Experimental Procedures

HeLa cells were maintained in Dulbecco's modified eagle's medium (DMEM) containing 5% fetal bovine serum, 3.7 g/L sodium bicarbonate, and 1% antibiotics. Cells treated with MNNG at two concentrations of 50 and 100 μM were maintained in the incubator at 37°C. An aliquot of 5 mM pyruvate and 10 mM glucose were added into fresh medium after the washout of 100 μM MNNG treatment for 30 min.

2.2 Immunocytochemistry

Treated cells were fixed with 4% paraformaldehyde and then made permeable by 0.2% Triton X-100 at room temperature after being washed twice with phosphate buffer solution (PBS). Cells were blocked with 1% bovine serum albumin (BSA) at 37°C for 30 min and then incubated with an anti-poly(ADP-ribose) (pADPr) (10H, Santa Cruz, Delaware, California) antibody at room temperature in the dark for 2 h followed by extensive washing with PBS. Cells were incubated with fluores-

cein isothiocyanate-conjugated anti-mouse antibody (Novus Biologicals, Littleton, Colorado) at room temperature for 60 min. Cell images were taken on a microscope with the fluorescence imaging system (EPIPHOT200, Nikon, Melville, New York).

2.3 Nicotinamide Adenine Dinucleotide/ Reduced Nicotinamide Adenine Dinucleotide Quantification Assay

The NAD⁺/NADH levels in the HeLa cells receiving different treatments were measured using a Bio-Vision NAD⁺/NADH quantification assay kit according to manufacture instructions (Biovision, Mountain View, California). A standard curve generated with known amounts of purified NADH was used to calculate the NAD⁺ and NADH concentrations, respectively, in the cells.

2.4 Measurement of Intracellular Adenosine-5'-triphosphate Level

Intercellular ATP level was measured by the bioluminescent somatic cell ATP assay kit (Sigma-Aldrich, St. Louis, Missouri).²⁰ Cells were collected at different time points after MNNG treatment. An aliquot of 50 μl of viable cell suspension was mixed with 150 μl of somatic cell releasing buffer to release the intercellular ATP. Half of the mixture (i.e., 100 μl) was then transferred into a black OptiPlate-96F 96-well plate containing 100 μl of ATP assay mix in each well. The luminescence intensity was measured by using the Victor² 1420 Multilabel Counter (PerkinElmer, Waltham, Massachusetts). The luminescence intensity was normalized to the number of cells.

2.5 Measurement of Mitochondrial Membrane Potential

The mitochondrial membrane potential ($\Delta\Psi$) of HeLa cells was determined by the fluorescence dye 5,5',6,6'-tetrachloro-1,1';3,3'-tetraethylbenzimidazolyl carbocyanine iodide (JC-1; Molecular Probes, Carlsbad, California) as our previous study and others.^{21,22} Cell pellet was loaded with a fresh medium containing 2 μM JC-1 for 30 min at 37°C. Cells were then washed twice with PBS, resuspended in 200 μl PBS, and transferred into a black OptiPlate-96F 96-well plate to measure $\Delta\Psi$ by the Victor² 1420 Multilabel Counter (PerkinElmer, Waltham, Massachusetts). J-monomer fluorescence was excited and emitted at 485 and 535 nm, respectively. J-aggregate fluorescence was excited and emitted at 544 and 590 nm, respectively. The $\Delta\Psi$ was determined by the ratio of J-aggregate/J-monomer.²³

2.6 Cell Viability Assay

The MTT (3-(4,5-dimethylthiazolyl-2)-2,5-diphenyltetrazolium bromide) assay was used for cell viability after different treatments. The treatment medium had been replaced with serum-free medium containing 0.2 mg/ml MTT, and the cells were incubated for 3 h at 37°C. After incubation, the MTT solution was discarded and 200 μl of DMSO was added. The extraction process was performed for 10 min at 37°C. The optical density (OD) was then recorded at 570 nm using the Varioskan Flash (Thermo Scientific, Waltham, Massachusetts). The mean

OD of the control cells represents 100% of the viability, and the results are expressed as a percentage of the control.

2.7 Measurement of the Respiration Rate

The cell respiration rate was measured by 782 Oxygen Meter (Mitocell MT200A, Strathelvin Instrument, Motherwell, United Kingdom) as previously reported.^{20,24} An aliquot of 4×10^5 cells was resuspended in 330 μl of assay buffer (125 mM sucrose, 65 mM KCl, 2 mM MgCl₂, 20 mM phosphate buffer, pH 7.2) and the cell suspension was transferred into the respiration chamber. An aliquot of 0.0004% digitonin was added to make the outer membrane of mitochondria permeable. The substrate-supported respiration rate was measured after 17 mM glutamate and 17 mM malate were injected into the chamber, and the State 3 respiration (the state of ATP synthesis) was then recorded after injection of 1.5 mM ADP. The acceptor control ratio (ACR) was calculated by dividing the State 3 respiration rate by the substrate-supported respiration rate. ACR differs from more commonly measured respiratory control ratio but can still reflect the mitochondrial coupling strength.²⁵

2.8 Reduced Nicotinamide Adenine Dinucleotide Fluorescence Lifetime Image

NADH fluorescence lifetime images of HeLa cells were obtained as previously described.^{18,19} In brief, treated HeLa cells were imaged with a two-photon laser scanning microscope and with a 60×1.45 NA PlanAchromat oil objective lens (Olympus Corp., Tokyo, Japan). NADH fluorescence was excited at 740 nm by a Verdi pumped modelocked femtosecond Ti:sapphire laser (Coherent, Inc., Santa Clara, California) at 76 MHz and the emitted fluorescent light was detected at 447 ± 30 nm, the NADH fluorescence peaks by a bandpass filter (Semrock Inc., Rochester, New York). Fluorescence photons were detected by a photon-counting photomultiplier H7422P-40 (Hamamatsu Photonics K.K., Hamamatsu, Japan). Time-resolved detection was conducted by the time-correlated single photon counting SPC-830 board (Becker & Hickl GmbH, Berlin, Germany). Data were analyzed with the commercially available SPCImage v2.8 software (Becker & Hickl GmbH, Berlin, Germany) via a convolution of the two component exponential decay function, $F(t) = a_1 e^{-t/\tau_1} + a_2 e^{-t/\tau_2}$ and the instrument response function (IRF), and were then fitted to the actual data to lifetime parameters τ_1 , τ_2 , a_1 , a_2 , and τ_m . τ_m is the mean lifetime defined as $(a_1 \tau_1 + a_2 \tau_2)/(a_1 + a_2)$. IRF was measured using a second harmonic generated signal from a periodically poled lithium niobate crystal. HeLa cells were seeded onto a 24-mm diameter glass coverslips (Paul Marienfeld GmbH & Co., Lauda-Königshofen, Germany) at 2×10^4 cells/cm² 24 h before fluorescence lifetime measurement and drug treatment. The coverslip was washed twice using PBS and then transferred into an imaging chamber and added 1 ml aliquot of 5 mM 4-(2-hydroxyethyl)-1-piperazineethanesulfonic acid (HEPES) buffer (5 mM KCl, 140 mM NaCl, 2 mM CaCl₂, 1 mM MgCl₂, 10 mM glucose, pH 7.4) in the beginning of fluorescence lifetime imaging.

2.9 Measurement of Reduced Nicotinamide Adenine Dinucleotide Fluorescence Intensity

NADH fluorescence intensity is measured by using a commercial fluorescence spectroscopy system (Victor² 1420 Multilabel Counter, PerkinElmer, Waltham, Massachusetts). Treated cells of $\sim 4 \times 10^5$ were resuspended in 200 μl PBS and transferred into a black OptiPlate-96F 96-well plate (Packed Bioscience, PerkinElmer, Waltham, Massachusetts) to measure NADH fluorescence excited and emission at 355 and 460 nm. The process was done as soon as possible to prevent NADH degraded at room temperature and the measured value of the NADH fluorescence intensity was normalized to the cell number.

3 Results

3.1 *N*-methyl-*N'*-nitro-*N*-nitrosoguanidine Induced Significant Nicotinamide Adenine Dinucleotide Depletion but Less Reduced Nicotinamide Adenine Dinucleotide Depletion

MNNG induced cell death by activating PARP-1 that subsequently consumed NAD⁺ and adenosine 5'-diphosphate (ADP) through the ADP-ribosylation.^{4,6,9,26} We measured the effect of MNNG treatment on intracellular levels of NAD⁺ and NADH to confirm the depletion of NAD⁺ reported by several studies^{4,6,9} and to investigate if NADH is affected in a similar manner. As shown in Fig. 1(A) (open square), MNNG induced significantly rapid depletion of cellular NAD⁺, which was almost diminished 5 min after treatment with 100 μM MNNG. The cellular NADH level decreased less severely than NAD⁺ that NADH fell to 50% of the controls 5 min after MNNG induction from 88 ± 19 to 44 ± 2 pmol per 10^6 cells [Fig. 1(A), solid circle]. At 60 min after MNNG treatment, the cellular NADH further decreased to 31 ± 9 pmol per 10^6 cells. We also performed the measurements of NADH fluorescence intensity [Fig. 1(B)], which has been used as the optical biomarker of mitochondrial NADH.²⁷ Figure 1(C) compares the results using both methods and the same time-dependent decrease of NADH was observed. This result indicates that the NADH fluorescence intensity was well correlated with the cellular NADH content. Finally, the dynamic PARP-1 activation shown in Fig. 1(D) indicates that massive expression of PAR protein immediately appeared in the nucleus of HeLa cells after MNNG treatment and then significantly decreased at 30 min and disappeared at 60 min. The immediate decrease of NAD⁺ and NADH 5 min after MNNG induction seems associated with this immediate PARP-1 activation at the same time point.

3.2 Reduced Nicotinamide Adenine Dinucleotide Fluorescence Lifetime Increased After Poly(adenosine-5'-diphosphate-ribose) polymerase-1 Induced Cell Death in a Dose-dependent Manner

Figure 2 shows the representative time course micrographs of NADH fluorescence lifetime from the same field of view (FOV) of HeLa cells before and after 100 μM MNNG treatment [Fig. 2(A) (a)–(e)] and the corresponding normalized lifetime histograms [Fig. 2(A) (f)]. Fluorescence signals in the cytoplasm display the punctuate perinuclear pattern, which is attributed to mitochondria-associated NADH.¹⁹ Each pixel represents the

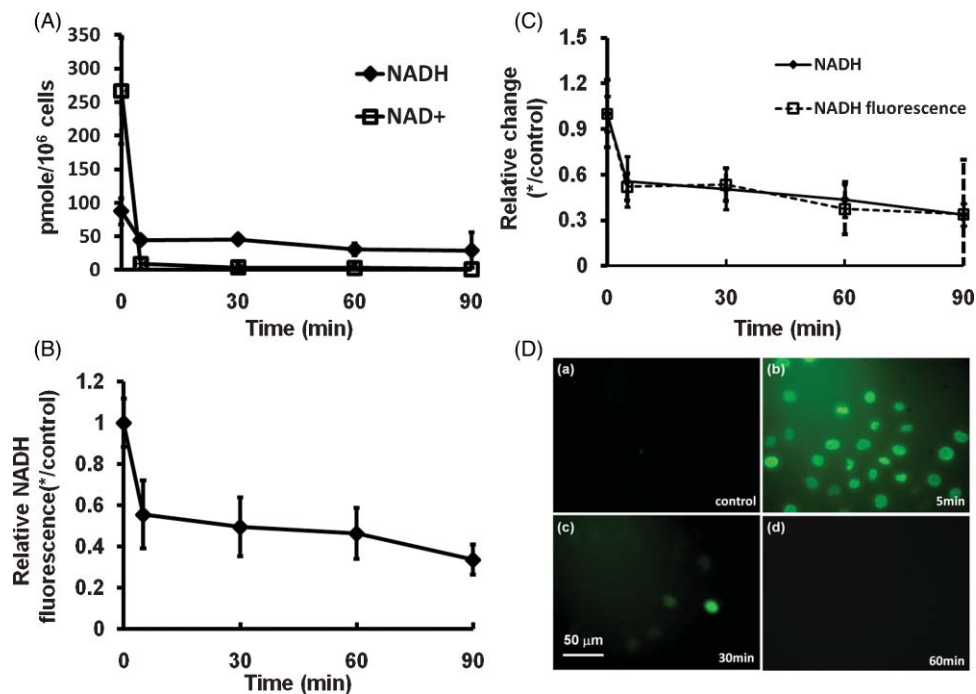


Fig. 1 Time course measurements of (A) cellular NAD⁺ and NADH content and (B) relative NADH fluorescence intensity to the control after 100 μM MNNG treatment. (C) Comparison of (A) and (B) by normalizing (A) to the control value. (D) Immunofluorescent images of anti-pADPr (a) before, and (b) 5, (c) 30, and (d) 60 min after 100 μM MNNG treatment. The scale bar in (c) is 50 μm .

mean lifetime (τ_m) of the short (τ_1) and long (τ_2) lifetime components weighted by their relative contributions a_1 and a_2 , respectively, such that $\tau_m = (a_1\tau_1 + a_2\tau_2)/(a_1 + a_2)$. The blue color in the color bar represents the longer lifetime (maximum 2000 ps) and the red color presents the shorter lifetime (minimum 500 ps). The color-coded lifetime images exhibit gradual color change from yellow to green and then blue from the image taken at the time point of controls to that taken 90 min after MNNG treatment. The normalized histograms of the mean lifetime (τ_m) from all pixels of the same FOV images taken at different time points show a peak shift from ~ 950 to ~ 1300 ps. The full-width-at-half-maximum is ~ 300 ps at the time of the control but becomes ~ 700 ps at 90 min after MNNG treatment indicating that the inhomogeneous lifetime distribution within cells varied greatly with time.

Similar results were repeatedly observed in a total of five samples at each time point and the average results are plotted in Fig. 2(B). In Fig. 2(B), the average results from cells treated with 50 μM MNNG are plotted to compare the MNNG dose effect. Figure 2(B) shows that NADH fluorescence lifetime increased up to 90 min after treatment with both MNNG doses. The increases at 30, 60, and 90 min are statistically significant (p -value < 0.05). The amplitude of the lifetime increase is dose-dependent that higher MNNG dose shows a higher increase in NADH fluorescence lifetime. Figure 2(C) plots the cell survival measured at 2 and 12 h after the treatment showing that 100 μM MNNG induced more cell death than did 50 μM . This dose dependent manner has been observed in our previous studies on STS-induced cell death of HeLa cells and cybrids with mitochondrial dysfunction, in which the faster the cell death proceeded, the higher NADH fluorescence lifetime increased.

3.3 Reduced Nicotinamide Adenine Dinucleotide Fluorescence Lifetime Increased Before Mitochondrial Dysfunction

Because NADH fluorescence is mainly attributed by the mitochondrial NADH, we examined the time course mitochondrial functions during PARP-1-mediated cell death to understand the possible origin of NADH fluorescence lifetime change observed in Fig. 2. We measured the mitochondrial membrane potential ($\Delta\Psi$) for up to 8 h and the intracellular ATP level for up to 2 h after treatment with both 50 and 100 μM MNNG, respectively, as shown in Fig. 3. Similar to the previously published result in HeLa cells,²⁶ $\Delta\Psi$ increased in the beginning of the MNNG treatment [Fig. 3(a), solid square] due to short supply of ADP in mitochondrial State 4 respiration,²⁸ and ATP dropped to 10% or more after treatment with 100 μM MNNG for 30 min [Fig. 3(b), solid square]. Both changes were dose-dependent as revealed by the observation that ATP was depleted more severely and faster and $\Delta\Psi$ reached the plateau earlier by treating HeLa cells with 100 μM MNNG compared with 50 μM MNNG. Compared to Fig. 2, the increase of NADH fluorescence lifetime occurred in parallel with the $\Delta\Psi$ raise and ATP depletion.

We further investigated the mitochondrial respiration rate and the coupling strength. The upper panel of Table 1 shows the substrate-supported oxygen consumption rate and State 3 respiration of 100 μM MNNG-treated HeLa cells. Both the substrate-supported respiration and State 3 respiration significantly decreased after MNNG exposure for 30, 60, and 120 min as compared to the controls. The mitochondrial coupling strength, indicated by the so-called ACR which was the ratio between the rate of State 3 respiration and substrate-supported respiration

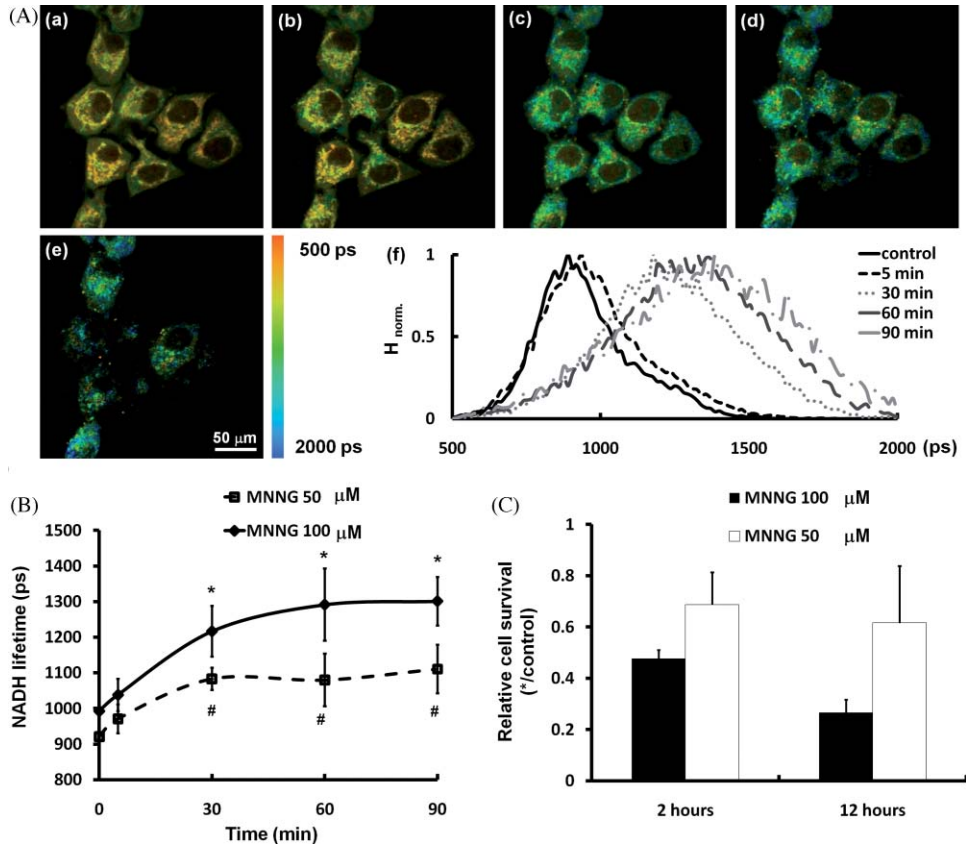


Fig. 2 (A) Two-photon fluorescence lifetime imaging (FLIM) micrographs of HeLa cells from the same sites (a) before, and (b) 5, (c) 30, (d) 60, and (e) 90 min after treatment with 100 μM MNNG. The normalized histograms of NADH fluorescence lifetime (f) over each 256×256 pixel lifetime image shown in (a) to (e) were plotted and coded with different colors. (B) Time course plots of the mean and standard deviation of NADH fluorescence lifetime over five fields of view of HeLa cells with 50 μM (open square) or 100 μM (solid diamond) MNNG treatment. Symbols * and # indicate the lifetime is significantly different from the value of the control with a *p*-value less than 0.05. (C) Relative cell survival to the control at 2 and 12 h after 30-min treatment with 50 μM (open square) or 100 μM (solid square) MNNG.

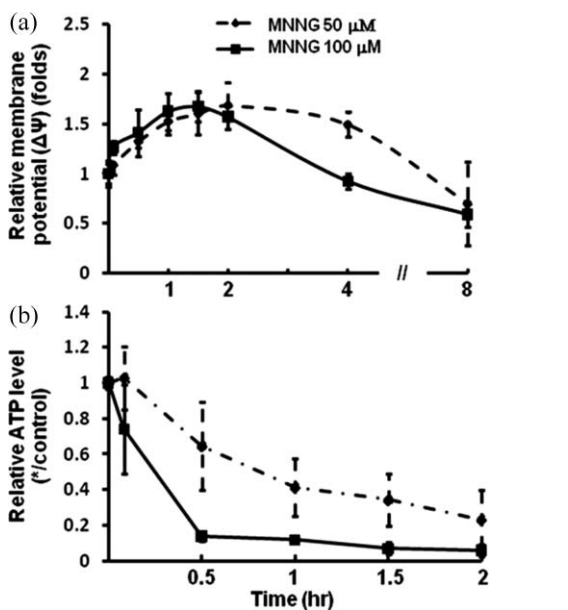


Fig. 3 Time course plots of (a) the relative mitochondrial membrane potential ($\Delta\Psi$) and (b) relative ATP level to the control before and after 50 μM (♦) or 100 μM (solid square) MNNG treatment.

rate,²⁵ was not observed at 30 and 60 min but was significantly decreased at 120 min after MNNG treatment (*p*-value = 0.007), indicating the compromise of mitochondrial respiration.

3.4 *N*-methyl-*N'*-nitro-*N*-nitrosoguanidine-induced Cell Death is Rescued by Pyruvate but not Glucose

NAD⁺ and ADP/ATP depletion induced by PARP-1 hyperactivation inhibited glycolysis and mitochondrial respiration.^{9,12,26} After washout of 100 μM MNNG exposure for 30 min, we treated cells with pyruvate or glucose to investigate whether MNNG induced cell death was rescued. We compared the survival rate of HeLa cells treated with these two substrates with that of addition of DMEM, instead of metabolic substrates. As shown in Fig. 4(a), the survival rate was not improved by addition of DMEM, which was 48 ± 3% and 27 ± 5% at 2 and 12 h, respectively, after treatment with 100 μM MNNG for 30 min. The survival rate was significantly increased by pyruvate to become 62 ± 8% (*p*-value = 0.007) and 36 ± 7% (*p*-value = 0.042) at 2 and 12 h time points, respectively. However, it was not changed by glucose (*p*-values = 0.071 and 0.172, respectively).

Table 1 The substrate-supported oxygen consumption rate and State 3 respiration rate of HeLa cells, which were treated by 100 μM MNNG for up to 120 min, or treated by metabolic substrate (i.e., glucose or pyruvate) or only culture medium after 100 μM MNNG treatment for 30 min, were measured at various time points by adding substrates of glutamate/malate and glutamate/malate plus ADP, respectively. The coupling effect was reflected via the ACR that was determined by the ratio of State 3 respiration rate divided by the substrate-supported oxygen consumption rate.

	Substrate-supported (nmole/min/ 10^6 cells)	State 3 (nmole/min/ 10^6 cells)	ACR	<i>n</i>
Control	3.8 ± 0.4	5.7 ± 0.6	1.5 ± 0.1	6
+ MNNG 30 min	2.9 ± 0.4^a	4.2 ± 0.7^a	1.4 ± 0.1	6
+ MNNG 60 min	1.9 ± 0.2^a	3.0 ± 0.1^a	1.6 ± 0.2	3
+ MNNG 120 min	2.1 ± 0.2^a	2.6 ± 0.2^a	1.3 ± 0.1^a	4
Post MNNG 30 min				
+ DMEM 30 min	3.0 ± 0.3^a	4.4 ± 0.6^a	1.5 ± 0.2	4
+ glucose 30 min	2.4 ± 0.6^a	3.7 ± 0.3^a	1.5 ± 0.2	5
+ pyruvate 30 min	4.4 ± 0.5^b	6.4 ± 0.9^b	1.5 ± 0.1	3

^a $p < 0.05$ compared with the control.

^b $p < 0.05$ compared with 30-min MNNG plus 30-min DMEM treatment.

We then measured the mitochondrial functions, including $\Delta\Psi$, ATP level, and the rates of oxygen consumption of cells in DMEM, pyruvate, or glucose exposure for 30 min after the washout of 30 min MNNG exposure. The results are shown in Figs. 5(a) and 5(b) and the bottom panel of Table 1. In Fig. 5, the experiment to treat cells with MNNG only for 60 min was added so that all of the measurements were compared at the same time point (i.e., 60 min from the beginning of 100 μM MNNG treatment). Addition of pyruvate or glucose did prevent the increase of $\Delta\Psi$ as compared with conditions of treating with MNNG for 60 min or treating with MNNG for 30 min plus DMEM for another 30 min that the relative membrane potentials to the controls were 1.54 ± 0.22 and 1.27 ± 0.08 (p -values < 0.05), respectively. In the measurement of the relative ATP level [Fig. 5(b)], pyruvate restored the relative ATP from $11.7 \pm 1.3\%$ to $19.4 \pm 0.7\%$ in cells exposed to 1-h MNNG treatment (p -value < 0.05) and from $16.6 \pm 0.1\%$ for 30 min MNNG plus 30 min DMEM exposure (p -value < 0.05). However, glucose

was unable to prevent ATP depletion at all. In the measurement of the oxygen consumption rate (Table 1), addition of pyruvate significantly improved both substrate-supported and State 3 respiration rates. The substrate-supported respiration rate increased from 1.9 ± 0.2 nmole/min/ 10^6 cells for 60 min MNNG treated cells or from 3.0 ± 0.3 nmole/min/ 10^6 cells for 30 min MNNG plus 30 min DMEM treated cells to 4.4 ± 0.5 nmole/min/ 10^6 cells. The State 3 respiration rate was increased from 3.0 ± 0.1 nmole/min/ 10^6 cells for 60-min MNNG treatment only or 4.4 ± 0.6 nmole/min/ 10^6 cells for 30 min-MNNG treatment plus 30 min DMEM to 6.4 ± 0.89 nmole/min/ 10^6 cells. Similarly to the findings of ATP levels, glucose did not restore oxygen consumption rates.

3.5 Reduced Nicotinamide Adenine Dinucleotide Fluorescence Lifetime Responded to Pyruvate but not Glucose; Reduced Nicotinamide Adenine Dinucleotide Fluorescence Intensity Responded to Neither Pyruvate nor Glucose

Figures 5(c) and 5(d) show the NADH fluorescence intensity and lifetime, respectively, of HeLa cells treated with 30 min DMEM, pyruvate, or glucose after washout of 30 min MNNG exposure. An additional measurement at 60 min after MNNG treatment was included in both Figs. 5(c) and 5(d) for comparison. The NADH fluorescence intensity was expressed as the value relative to the controls. The mean value of NADH fluorescence lifetime of the controls shown in Fig. 2(B) (i.e., 993 ± 30 ps) is depicted by a dashed line in Fig. 5(d). The NADH fluorescence intensity of HeLa cells with different treatments shows no difference. On the other hand, the NADH fluorescence lifetime, similar to the results in Fig. 2(B), increased to 1215 ± 28 ps after cells had been exposed to MNNG for 30 min plus 30 min incubation in DMEM and increased to 1291 ± 102 ps after cells exposed to 60 min MNNG. Pyruvate significantly prevented the NADH fluorescence lifetime increase, and after pyruvate treatment the

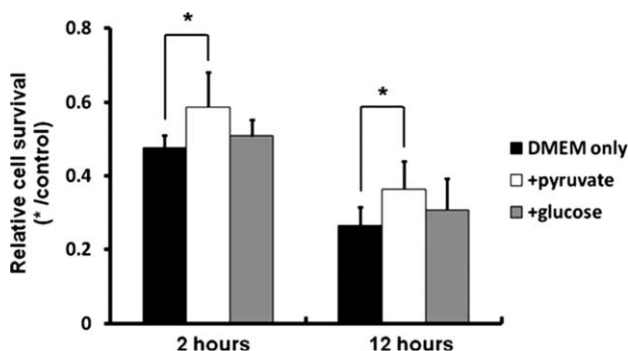


Fig. 4 Relative cell survival of HeLa cells treated with pyruvate (white bar) or glucose (gray bar), or without any substrate (i.e., DMEM only) (black bar) at 2 and 12 h after 30 min treatment with 100 μM MNNG. The symbol * indicates two values are significantly different with a p -value less than 0.05.

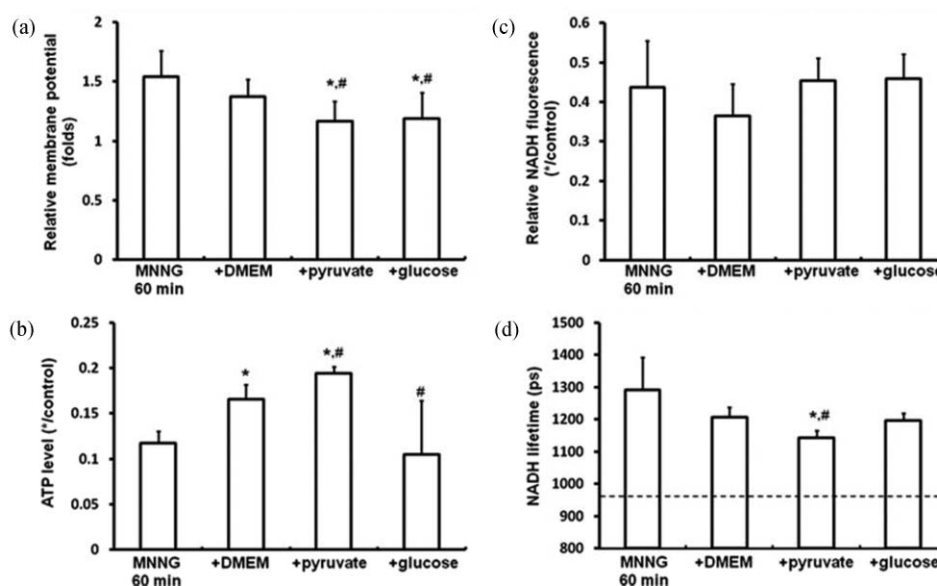


Fig. 5 Change of (a) the mitochondrial membrane potential ($\Delta\Psi$), (b) ATP level, (c) NADH fluorescence intensity, and (d) NADH fluorescence lifetime after 60-min 100 μM MNNG treatment, or 30-min 100 μM MNNG treatment followed by either 30 min pyruvate, glucose, or DMEM only treatment. Symbols * and # indicate the value is significantly different (p -value < 0.05) from the value of the 60-min MNNG treatment and 30-min MNNG plus 30-min DMEM treatment, respectively. The dotted line shown in (d) indicates the NADH fluorescence lifetime of HeLa cells before any treatment (the control).

lifetime (i.e., 1142 ± 23 ps) was different from that without addition of pyruvate (i.e., p -values = 0.008 and 0.002 for 60 min-MNNG treatment and 30 min MNNG plus 30 min DMEM, respectively). Glucose did not alter the lifetime increase and the lifetime (1197 ± 21 ps) was not statistically different from that of the cells treated with MNNG for 30 min plus 30 min incubation in DMEM.

4 Discussion

The first goal of this study was to identify if the NADH fluorescence lifetime responded to PARP-1-mediated cell death. The results of this study show a significant increase of NADH fluorescence lifetime after PARP-1 was hyperactivated by MNNG for up to 90 min [Fig. 2(A)]. Similar to our previous findings in STS-induced cell death, this increase of NADH fluorescence lifetime was dose-dependent in that the earlier the cell death started [Fig. 2(C)] the higher the NADH fluorescence lifetime increased [Fig. 2(B)]. During this lifetime increase, mitochondrial membrane potential $\Delta\Psi$ shows an increase as well for up to 90 min at a higher dose (100 μM) or 2 h at a lower dose (50 μM) and then decreased [Fig. 3(a)]. The increase of $\Delta\Psi$ was caused by a shortage of ADP because it was consumed to form PAR when PARP-1 was activated.²⁸ The Complex V in the mitochondria lacked ADP for ATP synthesis and resulted in the proton accumulation across the mitochondrial membrane and increased $\Delta\Psi$.²⁶ Similar to other published results,^{4,26} ATP was significantly depleted immediately and decreased to less than 20% after treatment with 100 μM MNNG for 30 min [Fig. 3(b)]. The electron transport chain was expected to slow down or be blocked that was revealed by decreased oxygen consumption rates (Table 1). Mitochondrial uncoupling did not appear until 120 min after 100 μM MNNG treatment, in which the ACR

value (i.e., 1.3 ± 0.1) was significantly lower than that of the control (i.e., 1.5 ± 0.1) (p -value = 0.007). These time course results of mitochondrial functions confirmed that the NADH fluorescence lifetime increased before diminishment of $\Delta\Psi$ and mitochondrial uncoupling.

Our second goal was to investigate if the NADH fluorescence intensity and/or lifetime responded to the treatment of cells with pyruvate or glucose. Our results show that the NADH fluorescence lifetime, not intensity, responded to pyruvate treatment [Figs. 5(c) and 5(d)]. It was demonstrated that neither glucose nor DMEM alone caused the lifetime decrease or recovery toward the value of controls [Fig. 5(d)]. In the measurements of mitochondrial functions and cell viability, we found that pyruvate increased the ATP level [Fig. 5(b)], oxygen consumption rate (Table 1, lower panel), and cell viability (Fig. 4) as compared to the DMEM and glucose treatments after MNNG washout. Furthermore, pyruvate prevented the increase of $\Delta\Psi$ [Fig. 5(a)], indicating the resumption of the electron transport chain. However, glucose also shows the same effect on $\Delta\Psi$. Because the ATP level and oxygen consumption rate decreased further after glucose treatment, we suggest that this decrease of $\Delta\Psi$ is the sign of cells being informed to die instead of being rescued from death. In fact, Fig. 4 shows that glucose did not improve the cell viability as compared to the cells exposed to DMEM after a 30-min MNNG treatment. Ying et al. also showed that cell survival was not improved by glucose in astrocytes after MNNG treatment.⁹

The conditions of a 30-min MNNG treatment with or without additional 30 min incubation in DMEM are comparable. The results show no significant difference in the values of oxygen consumption rate, $\Delta\Psi$, and ATP level between these two conditions. As presented in Table 1, the substrate-supported respiration rates were 2.9 ± 0.4 versus

3.0 ± 0.3 nmole/min/ 10^6 cells and the State 3 respiration rates were 4.2 ± 0.7 versus 4.4 ± 0.6 nmole/min/ 10^6 cells for the conditions without and with DMEM, respectively. While comparing the 30-min MNNG treatment with DMEM with the 60-min MNNG treatment, $\Delta\Psi$ shows less increase and ATP shows less depletion [Figs. 5(a) and 5(b)]. The $\Delta\Psi$ and ATP values of the cells treated with MNNG for 30 min followed by incubation with DMEM are comparable to those data in Figs. 3(a) and 3(b) measured at 30 min (i.e., $\Delta\Psi$ and ATP relative to the controls are 1.41 ± 0.23 and $13.7 \pm 2.9\%$, respectively).

The mechanism of PARP-1-mediated cell death has been well studied and it was proposed that significant NAD^+ and ADP depletion resulted in the energy failure. However, little is known about the role of NADH. In one study, the NADH fluorescence was measured before and after the addition of rotenone, a Complex I inhibitor, during the PARP-1-mediated cell death.²⁶ NADH was increased after rotenone was added, indicating that PARP-1 only depleted NAD^+ but not NADH. In this study, we measured the NADH using a NAD^+/NADH quantification assay for intracellular NADH [Fig. 1(A)] and NADH fluorescence intensity [Fig. 1(B)]. Different from NAD^+ that almost vanished from its control value ~ 260 pmole/ 10^6 cells after MNNG induction, cellular NADH dropped $\sim 50\%$ from ~ 100 to ~ 50 pmole/ 10^6 cells within the first 5 min and stayed stable afterward [Fig. 1(A)]. The NADH fluorescence intensity shows almost an identical trend, indicating that the NADH fluorescence intensity well represents intracellular NADH content [Fig. 1(C)]. Because NADH fluorescence signals were mainly from mitochondria,²⁹ the results indicate that during extensive PARP-1 activation the intracellular NADH remained mainly in mitochondria. Treatment of cells with pyruvate and glucose did not affect the NADH fluorescence intensity [Fig. 5(c)]. Together with the results in Fig. 1(B) that NADH remained stable during PARP-1 hyperactivation, we suggest that these remaining and stable mitochondrial NADH after MNNG treatment may play a critical role to be used once the electron transport chain was resumed by TCA metabolites such as pyruvate.

The NADH fluorescence lifetime is attributed to the lifetime components τ_1 and τ_2 of the free and protein-bound NADH, respectively, and the relative contribution ratio (a_1 -to- a_2 ratio).^{18,30} The protein-bound NADH has a longer lifetime and thus dominates the overall NADH fluorescence lifetime change. Our previous study shows that both NADH fluorescence intensity and lifetime increased in the beginning of STS-induced cell death, and this increased lifetime was due to both the increase in protein bound NADH fluorescence τ_2 and decrease in free-to-bound NADH ratio (i.e., increased bound NADH contribution).¹⁹ The increase in τ_2 may be caused by a protein conformational change such as phosphorylation. The increase in the contribution of bound NADH is in part due to an increase of the NADH content (increased NADH fluorescence intensity) because it may increase the interaction between NADH and surrounding proteins in mitochondria. However, the decrease of NADH content found in this study after MNNG treatment did not alter the increase of the NADH fluorescence lifetime. This finding supports the notion that the increase in the NADH fluorescence lifetime is mainly due to increased protein-protein interaction, although the specific protein(s) involved was not identified in the experimental design of this study.

Acknowledgments

We acknowledge the use of the imaging core facility of National Yang-Ming University. This work was supported by the "Aim for Top University Plan" from the Ministry of Education of Taiwan and by Grant Nos. NSC94-2321-B-010-004-YC, NSC98-2312-M-010-003, and NSC97-2320-B-010-013-MY3 from the National Science Council of Taiwan.

References

1. D. D'Amours, S. Desnoyers, I. D'Silva, and G. G. Poirier, "Poly(ADP-ribose)ylation reactions in the regulation of nuclear functions," *Biochem. J.* **342**(2), 249–268 (1999).
2. P. H. Chan, "Reactive oxygen radicals in signaling and damage in the ischemic brain," *J. Cereb. Blood Flow Metab.* **21**(1), 2–14 (2001).
3. W. X. Zong, D. Ditsworth, D. E. Bauer, Z. Q. Wang, and C. B. Thompson, "Alkylating DNA damage stimulates a regulated form of necrotic cell death," *Genes Dev.* **18**(11), 1272–1282 (2004).
4. C. C. Alano, P. Garnier, W. Ying, Y. Higashi, T. M. Kauppinen, and R. A. Swanson, "NAD⁺ depletion is necessary and sufficient for poly(ADP-ribose) polymerase-1-mediated neuronal death," *J. Neurosci.* **30**(8), 2967–2978 (2010).
5. J. Zhang, V. L. Dawson, T. M. Dawson, and S. H. Snyder, "Nitric oxide activation of poly(ADP-ribose) synthetase in neurotoxicity," *Science* **263**(5147), 687–689 (1994).
6. W. Ying, Y. Chen, C. C. Alano, and R. A. Swanson, "Tricarboxylic acid cycle substrates prevent PARP-mediated death of neurons and astrocytes," *J. Cereb. Blood Flow Metab.* **22**(7), 774–779 (2002).
7. S. W. Yu, H. Wang, M. F. Poitras, C. Coombs, W. J. Bowers, H. J. Federoff, G. G. Poirier, T. M. Dawson, and V. L. Dawson, "Mediation of poly(ADP-ribose) polymerase-1-dependent cell death by apoptosis-inducing factor," *Science* **297**(5579), 259–263 (2002).
8. C. Szabo, "The pathophysiological role of peroxynitrite in shock, inflammation, and ischemia-reperfusion injury," *Shock* **6**(2), 79–88 (1996).
9. W. Ying, C. C. Alano, P. Garnier, and R. A. Swanson, "NAD⁺ as a metabolic link between DNA damage and cell death," *J. Neurosci. Res.* **79**(1–2), 216–223 (2005).
10. J. Zeng, G. Y. Yang, W. Ying, M. Kelly, K. Hirai, T. L. James, R. A. Swanson, and L. Litt, "Pyruvate improves recovery after PARP-1-associated energy failure induced by oxidative stress in neonatal rat cerebrocortical slices," *J. Cereb. Blood Flow Metab.* **27**(2), 304–315 (2007).
11. K. Zhu, R. A. Swanson, and W. Ying, "NADH can enter into astrocytes and block poly(ADP-ribose) polymerase-1-mediated astrocyte death," *NeuroReport* **16**(11), 1209–1212 (2005).
12. W. Ying, P. Garnier, and R. A. Swanson, "NAD⁺ repletion prevents PARP-1-induced glycolytic blockade and cell death in cultured mouse astrocytes," *Biochem. Biophys. Res. Commun.* **308**(4), 809–813 (2003).
13. Z. Zhang, D. Blessington, H. Li, T. M. Busch, J. Glickson, Q. Luo, B. Chance, and G. Zheng, "Redox ratio of mitochondria as an indicator for the response of photodynamic therapy," *J. Biomed. Opt.* **9**(4), 772–778 (2004).
14. H. W. Wang, Y. H. Wei, and H. W. Guo, "Reduced nicotinamide adenine dinucleotide (NADH) fluorescence for the detection of cell death," *Anticancer Agents Med. Chem.* **9**(9), 1012–1017 (2009).
15. J. R. Lakowicz, H. Szmajdzinski, K. Nowaczyk, and M. L. Johnson, "Fluorescence lifetime imaging of free and protein-bound NADH," *Proc. Natl. Acad. Sci. U.S.A.* **89**(4), 1271–1275 (1992).
16. D. K. Bird, L. Yan, K. M. Vrotsos, K. W. Eliceiri, E. M. Vaughan, P. J. Keely, J. G. White, and N. Ramanujam, "Metabolic mapping of MCF10A human breast cells via multiphoton fluorescence lifetime imaging of the coenzyme NADH," *Cancer Res.* **65**(19), 8766–8773 (2005).
17. Y. Wu, W. Zheng, and J. Y. Qu, "Sensing cell metabolism by time-resolved autofluorescence," *Opt. Lett.* **31**(21), 3122–3124 (2006).
18. H. W. Guo, C. T. Chen, Y. H. Wei, O. K. Lee, V. Gukassyan, F. J. Kao, and H. W. Wang, "Reduced nicotinamide adenine dinucleotide fluorescence lifetime separates human mesenchymal stem cells from differentiated progenies," *J. Biomed. Opt.* **13**(5), 050505 (2008).

19. H. W. Wang, V. Gukassyan, C. T. Chen, Y. H. Wei, H. W. Guo, J. S. Yu, and F. J. Kao, "Differentiation of apoptosis from necrosis by dynamic changes of reduced nicotinamide adenine dinucleotide fluorescence lifetime in live cells," *J. Biomed. Opt.* **13**(5), 054011 (2008).
20. C. T. Chen, Y. R. Shih, T. K. Kuo, O. K. Lee, and Y. H. Wei, "Coordinated changes of mitochondrial biogenesis and antioxidant enzymes during osteogenic differentiation of human mesenchymal stem cells," *Stem Cells* **26**(4), 960–968 (2008).
21. J. S. Yu, H. W. Guo, C. H. Wang, Y. H. Wei, and H. W. Wang, "Increase of reduced nicotinamide adenine dinucleotide fluorescence lifetime precedes mitochondrial dysfunction in staurosporine-induced apoptosis of HeLa cells," *J. Biomed. Opt.* **16**(3), 036008 (2011).
22. S. T. Smiley, M. Reers, C. Mottola-Hartshorn, M. Lin, A. Chen, T. W. Smith, G. D. Steele Jr., and L. B. Chen, "Intracellular heterogeneity in mitochondrial membrane potentials revealed by a J-aggregate-forming lipophilic cation JC-1," *Proc. Natl. Acad. Sci. U.S.A.* **88**(9), 3671–3675 (1991).
23. A. J. Woollacott and P. B. Simpson, "High throughput fluorescence assays for the measurement of mitochondrial activity in intact human neuroblastoma cells," *J. Biomol. Screening* **6**(6), 413–420 (2001).
24. Y. F. Chen, C. H. Kao, Y. T. Chen, C. H. Wang, C. Y. Wu, C. Y. Tsai, F. C. Liu, C. W. Yang, Y. H. Wei, M. T. Hsu, S. F. Tsai, and T. F. Tsai, "Cisd2 deficiency drives premature aging and causes mitochondria-mediated defects in mice," *Genes Dev.* **23**(10), 1183–1194 (2009).
25. R. Ventura-Clapier, A. Kuznetsov, V. Veksler, E. Boehm, and K. Anfous, "Functional coupling of creatine kinases in muscles: species and tissue specificity," *Mol. Cell Biochem.* **184**(1–2), 231–247 (1998).
26. G. Cipriani, E. Rapizzi, A. Vannacci, R. Rizzuto, F. Moroni, and A. Chiarugi, "Nuclear poly(ADP-ribose) polymerase-1 rapidly triggers mitochondrial dysfunction," *J. Biol. Chem.* **280**(17), 17227–17234 (2005).
27. J. Shimazaki, K. Tornheim, and R. A. Laing, "Correlation of redox fluorometry and analytical measurements of pyridine nucleotide," *Invest. Ophthalmol. Visual Sci.* **30**(10), 2274–2278 (1989).
28. A. Perl, P. Gergely Jr., G. Nagy, A. Koncz, and K. Banki, "Mitochondrial hyperpolarization: a checkpoint of T-cell life, death and autoimmunity," *Trends Immunol.* **25**(7), 360–367 (2004).
29. A. Mayevsky and G. G. Rogatsky, "Mitochondrial function in vivo evaluated by NADH fluorescence: from animal models to human studies," *Am. J. Physiol.: Cell Physiol.* **292**(2), C615–C640 (2007).
30. M. C. Skala, K. M. Riching, A. Gendron-Fitzpatrick, J. Eickhoff, K. W. Eliceiri, J. G. White, and N. Ramanujam, "In vivo multiphoton microscopy of NADH and FAD redox states, fluorescence lifetimes, and cellular morphology in precancerous epithelia," *Proc. Natl. Acad. Sci. U.S.A.* **104**(49), 19494–19499 (2007).